Lab on a Chip

Volume 1 | Number 1 | Jan 2013 | Pages 1–100

Lab on a Chip

Miniaturisation for chemistry, physics, biology, materials science and bioengineering
www.rsc.org/loc

ROYAL SOCIETY OF CHEMISTRY

ROYAL SOCIETY OF CHEMISTRY

www.rsc.org/loc

TOC Image and text for:

Chip-off-the-old-rock: The study of reservoir-relevant geological processes with real-rock micromodels

Wen Song, Thomas W. de Haas, Hossein Fadaei, and David Sinton
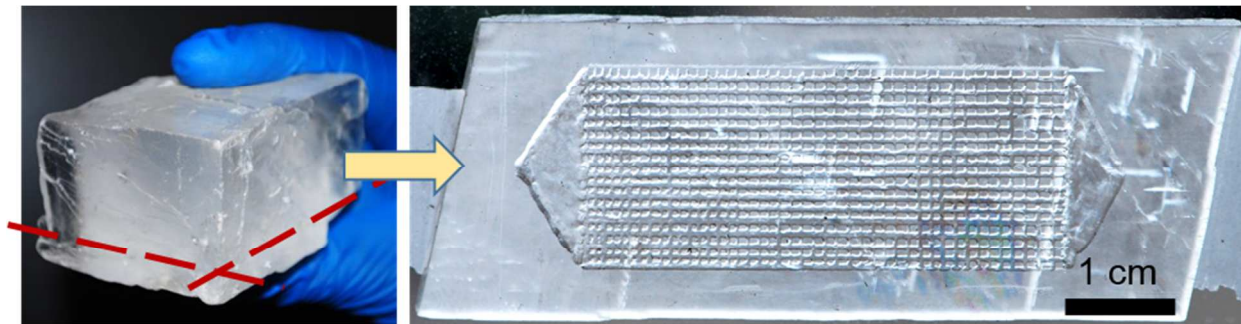
We present a geometrically and chemically representative real-rock micromodel for reservoir engineering studies; device fabrication and experimental results are presented.

PAPER

Chip-off-the-old-rock: The study of reservoir-relevant geological processes with real-rock micromodels

Wen Song,[a] **Thomas W. de Haas,**[b] **Hossein Fadaei,**[a] **and David Sinton*[a]**

We present a real-rock micromodel approach whereby microfluidic channels are fabricated in a naturally occurring mineral substrate. The method is applied to quantify calcite dissolution which is relevant to oil/gas recovery, CO_2 sequestration, and wastewater disposal in carbonate formations – ubiquitous worldwide. The key advantage of this method is the inclusion of both the relevant substrate chemistry 10 (not possible with conventional microfluidics) and real-time pore-scale resolution (not possible with core samples). Here, microchannels are etched into a natural calcite crystal and sealed with a glass slide. The approach is applied to study acidified brine flow through a single channel and a two-dimensional micromodel. The single-channel case conforms roughly to a 1-D analytical description, with crystal orientation influencing the local dissolution rate an additional 25%. The two-dimensional experiments 15 show highly flow-directed dissolution and associated positive feedback wherein acid preferentially invades high conductivity flow paths, resulting in higher dissolution rates ('wormholing'). These experiments demonstrate and validate the approach of microfabricating fluid structures within natural minerals for transport and geochemical studies. More broadly, real-rock microfluidics open the door to a vast array of lab-on-a-chip opportunities in geology, reservoir engineering, and earth sciences.
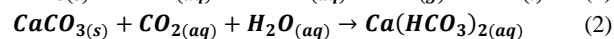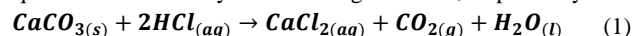
20

Introduction

Carbonate formations encompass both significant hydrocarbon deposits as well as deep saline aquifers suitable for carbon dioxide (CO_2) storage.[1–4] Carbonate reservoirs, namely limestones and 25 dolostones, account for more than 60% of global oil reserves and more than 40% of global natural gas reserves.[2] The Grosmont carbonate reservoir in Alberta, Canada, for example, contains 406 billion barrels (bbl) of original bitumen (extra heavy oil) in place.[5,6] Globally, more than 50% of currently accessible oil is contained in 30 Middle Eastern carbonate reservoirs, including the Ghawar and Kirkuk giant oil fields which are contained in limestone formations.[7,8] Combined CO_2-enhanced oil recovery and long-term CO_2 storage post-production in the carbonate layers of the Weyburn-Midale field currently comprise the largest CO_2 storage 35 project worldwide, and are predicted to extract an additional 155 million bbl of oil and store 30 million tonnes of CO_2 over 30 years.[9,10] However, carbonate reservoirs are highly heterogeneous, containing large voids as well as regions of poor connectivity and low permeability, making hydrocarbon extraction difficult.

40 In the petroleum industry, poor reservoir permeability and connectivity is enhanced through means of acid injection during secondary and tertiary recovery. One such process is acidizing, a method whereby brine with 1-15% hydrochloric acid (HCl) is injected into a carbonate reservoir to increase the connectivity of
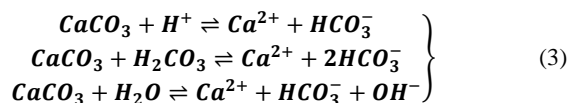
45 the pore space.[11–14] Acidic wastewater products are also injected into carbonate reservoirs in the form of flowback from hydraulically fractured reservoirs and blowdown (highly saline residual boiler water) from thermal recovery processes. Furthermore, deep carbonate reservoirs are preferred sites for CO_2 50 injection for long-term storage.[15] In such carbon sequestration efforts, acid dissolution of carbonates arises due to CO_2-acidification of formation water, post injection.[1,16–19] That is, CO_2 injection produces acid. In both storage efforts - waste disposal and CO_2 injection - formation dissolution due to acid flow, 55 especially at the pore scale, plays a key role in determining the storage capacity as well as likelihood for leakage, which directly impact the longevity and security of the well.

Pore-scale dynamics dictate the net flow behavior, and ultimately recovery or storage capacity of the reservoir. The 60 reactions between the carbonate rock (formally 'mineral') and the acidic fluids during (i) the acidizing process involving HCl, and (ii) the migration of CO_2-saturated brine through deep saline aquifers are dictated by the following reactions, respectively:

$$CaCO_{3(s)} + 2HCl_{(aq)} \rightarrow CaCl_{2(aq)} + CO_{2(g)} + H_2O_{(l)} \quad (1)$$

$$CaCO_{3(s)} + CO_{2(aq)} + H_2O_{(aq)} \rightarrow Ca(HCO_3)_{2(aq)} \quad (2)$$

While the chemistry of the two processes differ, both rely on the 65 same set of simultaneous reactions at the calcite crystal surface which dictate mineral dissolution, and the mechanistic changes in

the pore geometry and overall porosity (and hence permeability and subsequent flow behaviour) owing to carbonate matrix dissolution under acidic flows are comparable. The simultaneous reactions dictating the rate of calcite dissolution are as follows:

$$\left.\begin{array}{c} CaCO_3 + H^+ \rightleftharpoons Ca^{2+} + HCO_3^- \\ CaCO_3 + H_2CO_3 \rightleftharpoons Ca^{2+} + 2HCO_3^- \\ CaCO_3 + H_2O \rightleftharpoons Ca^{2+} + HCO_3^- + OH^- \end{array}\right\} \qquad (3)$$

Previous methods to quantify acid dissolution of carbonates have focused on core-based methods. While opaque to pore-scale dynamics, core studies do allow quantification of before-and-after properties such as permeability and porosity.[1,4,12,13,20] Techniques such as high-resolution optical profilometry (Elkhoury *et al.*, 2013), X-ray computed tomography (Nguyen *et al.*, 2013), and neutron radiography (Fredd and Fogler, 1998) have been applied to map initial and final core porosities as a result of carbonate matrix dissolution. These works are in agreement with respect to the increase in overall porosity and permeability due to fluid-solid reactions. However, the mechanisms dictating flow changes due to dissolution (i) at the pore level and (ii) in real time are not yet well understood.

Emerging methods for characterizing fluid-solid interactions at the pore-scale include chemically inert glass and silicon microfluidic devices which have been successfully applied to a range of applications in carbon management and reservoir engineering.[21–30] In particular, micromodels can achieve excellent geometric representation of rock pores to visualize reservoir fluid behaviour within various porous media.[23,25,29,30] Traditional micromodels cannot, however, capture the physical and geochemical fluid-rock interactions expected in rock. Specifically, wettability, pore-scale heterogeneities, and geochemical interactions are not replicated. Of particular interest with respect to carbonate reservoirs are the effects of carbonate dissolution as a result of acidic flow conditions, for example the time evolution of pore structure. Transparent calcite crystals are found up to several inches in size in a trigonal-rhombohedral structure. The transparent single-crystal nature of calcite lends itself readily to fabrication and optical interrogation methods germane to microfluidics. That is, calcite crystals present an opportunity for real-rock microfluidics, enabling the quantification of geochemistry and pore-scale fluid-rock interactions in real time.

In this paper, a real-rock micromodel approach is developed. Microfluidic channels are etched into a natural rock sample to visualize the dominant dissolution rates and patterns encountered during acidic flow through carbonate rocks. Calcite-based microfluidic platforms with two geometries were developed: (i) a single straight channel for one dimensional dissolution studies, and (ii) a porous medium composed of a square matrix for two-dimensional dissolution visualization. This method enables the direct visualization of the chemical and mechanical interactions between the native reservoir fluids, injected fluids, and the carbonate matrix at the pore and macro scales in real time.

Materials and methods

The pore-scale visualization of carbonate dissolution during acidic flows was achieved using a microfluidic device etched into a calcite crystal substrate. In this work, two flow geometries were fabricated: (i) a single, one dimensional channel to analyze carbonate dissolution over time, and (ii) a two dimensional network to quantify the effect of acidic flow on pore scale matrix dissolution in a geometrically and chemically representative micromodel. The one dimensional channel had an initial cross-sectional dimension of 500μm, typical of natural fracture apertures within carbonate reservoirs.[31] The two dimensional micromodel employed a matrix of square grains (initially ~ 500 μm x 500 μm) separated by initial channel widths of less than 300 μm. Although the presented micromodel geometry is primitive in comparison to a real carbonate rock, it is sufficient to demonstrate the visualization of pore-scale matrix dissolution dynamics. The fabrication process developed here (following section) is general and can be applied to reservoir-specific geometries in the future.

Fabrication of calcite microfluidic chip

Conventional microfabrication methods for glass and silicon are not applicable to calcite due to its highly reactive nature, and hence a new fabrication method was developed and is described here. The fabrication process for which microfluidic channels were etched into a thin calcite wafer is demonstrated in Fig. 1. First, a large calcite crystal was sectioned into 3mm thick wafers using a thin-sectioning saw (BUEHLER IsoMet 1000 Precision Saw) with a 7x0.025" diamond blade (BUEHLER IsoMet Wafering Blade 15 LC Diamond Sectioning 11-4277). The thin calcite wafer was subsequently ground smooth (Hillquist Thin Section Machine), cleaned with ethanol, and dried. The smoothed calcite surface ensured evenly etched features and proper bonding. The calcite wafer was dipped in a beaker of molten beeswax (CAS: 8012-89-3, Sigma-Aldrich) heated at 150°C and subsequently laid horizontally on a sheet of aluminum foil to solidify the thin wax layer. The aluminum foil separation layer was critical to allow contraction of the crystal upon cooling; cooling directly in contact with an unyielding solid substrate induced cracks. The wax coating on the calcite wafer was then smoothed using a sheet of 600 grain size sand paper (Norton Black Ice T214 Waterproof paper) to create a thin acid-resistant layer with homogeneous thickness. A layer on the order of hundreds of microns was sufficiently thick to mask the substrate while enabling full removal where desired. The desired microchannel pattern was removed from the wax film mask using a commercial CO_2 laser (30W Universal Laser Systems M-360). Optimal laser cutting was found to be a single pass at low power (5%) and low traverse speed (1%). These settings were sufficient to remove the wax, exposing the calcite where channels were desired with a minimum feature size of approximately 140 μm, while maintaining firm adhesion elsewhere.
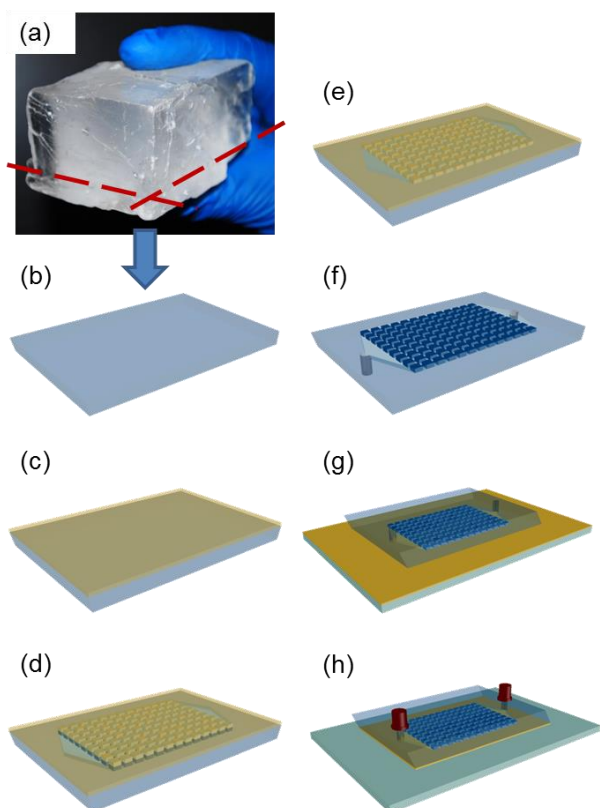
Fig. 1 Fabrication of the microfluidic flow channels in natural calcite material. A large calcite crystal (a) was cut into 3mm thick wafers (b) using a thin-sectioning saw, and coated with a thin layer of beeswax (c). The etching pattern was inscribed through the wax using a laser cutter (d), and the crystal was immersed in hydrochloric acid (HCl) to etch the desired pattern (e). Wax was removed from the etched crystal inlet and outlet holes were drilled (f). The cleaned etched surface was adhered to a clean glass side using a thin layer of adhesive (g), and nanoports were attached to allow for controlled flow (h).

The microfluidic features were etched by immersing the sealed calcite wafer in 10% hydrochloric acid (HCl) for 15 minutes such that the exposed channel patterns could be dissolved. The acid concentration was chosen to create smooth, uniform features in a controlled fashion within a reasonable timeframe. High concentrations of acid (greater than 10% HCl) resulted in violent gas evolution which caused the wax mask to detach from the calcite surface, and led to disproportionately etched features. Low concentrations of acid resulted in suitable features but long etch times. Furthermore, it is known that for pH less than 3.5, as in the case with the 10% HCl etchant, the dissolution reaction of calcite is mass transport limited.[32] In this regime, the activation energy required for dissolution is very low and the calcite is able to react readily. As such, the concentration of the dissolution products in the aqueous phase in close proximity to the crystal approaches the equilibrium concentration, and gives rise to smooth features (little to no etch pits seen as roughness along the channel).[32] To stop the etching process the calcite was submerged in deionized water. The substrate was then heated (150 °C) to melt away the bulk of the wax mask, followed by a rinse in cyclohexane to remove any remaining wax. Inlet and outlet holes were drilled through the

calcite wafer using a high speed drill press (Servo Products Company, Pasadena, CA) and a 1mm flat tip diamond grinding tool (McMaster Carr #4376A11). Holes were bored through the calcite side to accommodate the available visualization setup. The etched calcite wafer was rinsed with acetone followed by deionized water to remove drilling residues and provide a clean bonding surface. A thin layer of Scotch-Weld Instant Adhesive CA40 (McMaster Carr #75445A67) was applied to a 2x3" Scott D263T borosilicate glass slide before attaching to the etched calcite wafer. Excessive adhesive was wicked away prior to bonding to avoid plugging the microchannels due to strong capillary forces. The calcite was then clamped to the glass cover and left to seal. Two 1/16" Nanoports (IDEX Health & Science LLC, Oak Harbor, WA) were adhered to create an inlet and an outlet using Scotch-Weld DP-100 clear epoxy (McMaster Carr #7467A21). Once bonded, several pore volumes of acetone was flowed through the microfluidic system to remove any residual adhesive which may have adhered to the channel surface during bonding. Acetone is able to dissolve the adhesive without damaging the calcite crystal. The micromodel was rinsed with deionized water and dried before experimentation.

Experimental setup

The experimental setup is shown in Fig. 2. Deionized water was used to create a 1.81M sodium chloride (NaCl, CAS: 7647-14-5 BioShop Canada Inc., Burlington, ON, Canada) solution typical of formation brine. A black dye (Windsor & Newton Cotman WaterColors, Lamp Black 337 Series 1 AA, London, England) was added to the solution to enhance visualization contrast. The saline solution was acidified to 1% hydrochloric acid while stirred at atmospheric pressure to create a well-mixed, acidic brine typical of subsurface acidizing processes.
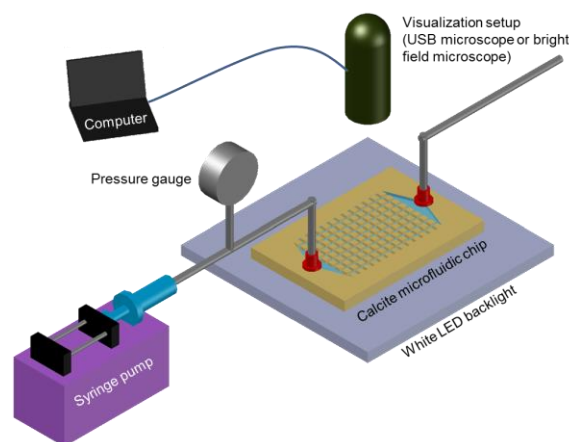

Fig. 2 Experimental setup for visualizing carbonate dissolution under acidic flow conditions. Acidic brine was injected using a syringe pump at a flow rate equivalent to near wellbore pore-scale velocities of 100m/day. The chip was open to atmosphere downstream. The calcite microfluidic device was imaged at the macroscale using a USB microscope (to obtain the porosity change over time) and at the microscale using a brightfield microscope.

The calcite micromodel was first filled with the colored brine under vacuum conditions and imaged to obtain the initial pore geometry. The 1% HCl brine was then loaded into a 60mL syringe (BD, Franklin Lakes, NJ) and a syringe pump (Harvard Apparatus,
5 Holliston, MA) was used to deliver the acidified brine at a constant flow rate corresponding to typical near-wellbore subsurface fluid velocity of 100 m/day for the flow experiments. The fluid velocity was chosen so as to match those of acidizing processes for reservoir stimulation used in industry. Constant flow rate was
10 selected in this test for practical reasons. Namely, flow rate control was dependable and consistent, whereas the formation and emergence of CO_2 bubbles disturbed the local pressure. In a porous network, both local pressure and flow rate conditions can vary with reservoir dynamics. The calcite microfluidic device was
15 maintained at atmospheric pressure downstream.

Pore scale matrix dissolution was visualized under bright field imaging using an inverted microscope (OLYMPUS CKX41). Matrix dissolution and subsequent porosity change over time at the macroscale were visualized using a USB microscope (Dinolite
20 Premier, AnMo Electronics Corporation, Taipei, Taiwan), with a white LED screen underneath the calcite micromodel to provide backlighting.

Results

The crystal structure of calcite enables the application of familiar
25 microfluidics fabrication methods, with some customization. Microchannels with dimensions on the order of hundreds of micrometers were laser-cut into the wax mask, subsequently employed to etch channels into the rock. The channel widths were ~ $(140 \mu m + 2 \cdot depth)$, in accordance with the minimum cutting
30 width of the laser cutter available. Fig. 3 shows a typical feature cross-sectional geometry. The smooth channel surfaces observed are indicative of a near equilibrium boundary layer (i.e., transport limited dissolution using the 10% HCl etchant solution) wherein the nucleation of pits is not energetically favorable and the
35 dissolution process occurs in stepwaves across the crystal surface.[32] In this regime, new steps only nucleate at the crystal edges. The channel shape thus depends on the channel orientation relative to the crystal plane. Unlike the uniformly isotropic etching common to glass microfluidics and uniformly crystallographic
40 etching common to silicon microfluidics, the channels created in the calcite wafer followed (i) a half-trapezoidal cross-sectional geometry parallel to the cleavage planes of the crystal on two surfaces (left wall and channel bottom in Fig. 3), typical of crystallographic etching, and (ii) a rounded edge on the side in
45 which the etching direction was orthogonal to the cleavage planes (right wall), typical of isotropic etching (as in glass microfluidic channels). The angle between the two crystallographically etched surfaces was consistently $\theta = 125° \pm 1°$; the radius of curvature of the isotropically etched wall, R, is on the order of the channel
50 depth, h. While the hybrid etched cross-section is atypical of microfluidics, it is a good representation of the variety of geometries expected in a natural calcite reservoir. In short, crystals are not aligned underground.
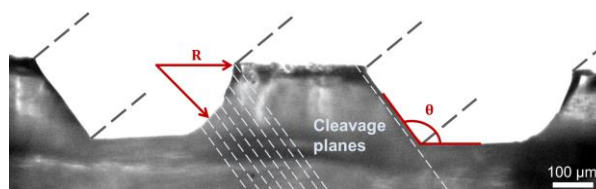

Fig. 3 Cross section of two-dimensional calcite matrix, showing crystallographic etching of features following the cleavage plane of the crystal as well as the isotropic-like etching on the side against the cleavage plane of the crystal (dissimilar to uniform isotropic etching in conventional glass- or silicon-based micromodels). Smooth features were created as a result of the near-equilibrium conditions in the fluid layer surrounding the crystal. The hybrid straight/curved etched cross-section is a good representation of the variety of geometries expected in a natural calcite reservoir.

55 Carbonate dissolution experiments were conducted at near-wellbore injection rates through calcite microfluidic chips. The two chip geometries were a single straight channel and a two-dimensional porous networks, or micromodel. Acidic brine with 1% HCl and 1.81M NaCl, typical of acidizing processes in
60 carbonate reservoirs, was injected through the calcite-based devices. Bright field imaging was performed at fixed locations throughout the course of the dissolution experiments. In both cases, several experiments (3 of each type) were conducted in which similar results were obtained.
65

Single microchannel experiments

To quantify the effect of fluid flux on dissolution, acidic brine was injected through a 500 μm wide straight channel at a constant flow rate corresponding to an initial near-well velocity of 100
70 m/day (1.16 mm/s). The channel was imaged at its midpoint (~15 mm from the entrance). The channels were fabricated with 3 cm lengths to be sufficiently long to avoid any end effects, and to accommodate for the calcite crystal sizes available. The time lapse video showing the channel widening over the course of the three
75 hour experiment is shown in the accompanying electronic supplementary information (ESI).

Fig. 4 shows the dynamics of the dissolution process. Over the course of the acid injection, CO_2 bubbles arising from the carbonate-acid reaction were observed. The gas phase consistently
80 nucleated at the channel corners and/or crystal defects along the channel wall. After nucleation, the bubbles grew in size, filling the cross-section of the channel, until bubble detachment. This process is illustrated in Fig. 4a with a dilute 0.1% HCl brine flow and relatively slow (2 m/day) pore velocity. The detachment
85 bubble length of ~600 μm was reached in ~ 13 min, and the process repeated continuously. In contrast, Fig. 4b shows the reservoir-relevant case of 1.0% HCl brine flow at 100 m/day pore velocity. The bubble formation and detachment process was rapid and chaotic, with a timescale on the order of ~ 10 s. Under these
90 conditions a combination of growth and coalescence was the norm.

(a)

t = 0 min   t = 6 min   t = 12 min

500 μm

t = 2 min   t = 8 min   t = 14 min

t = 4 min   t = 10 min   t = 16 min

(b)

t = 0 s   t = 4 s   t = 8 s

500 μm

t = 1 s   t = 5 s   t = 9 s

t = 2 s   t = 6 s   t = 10 s
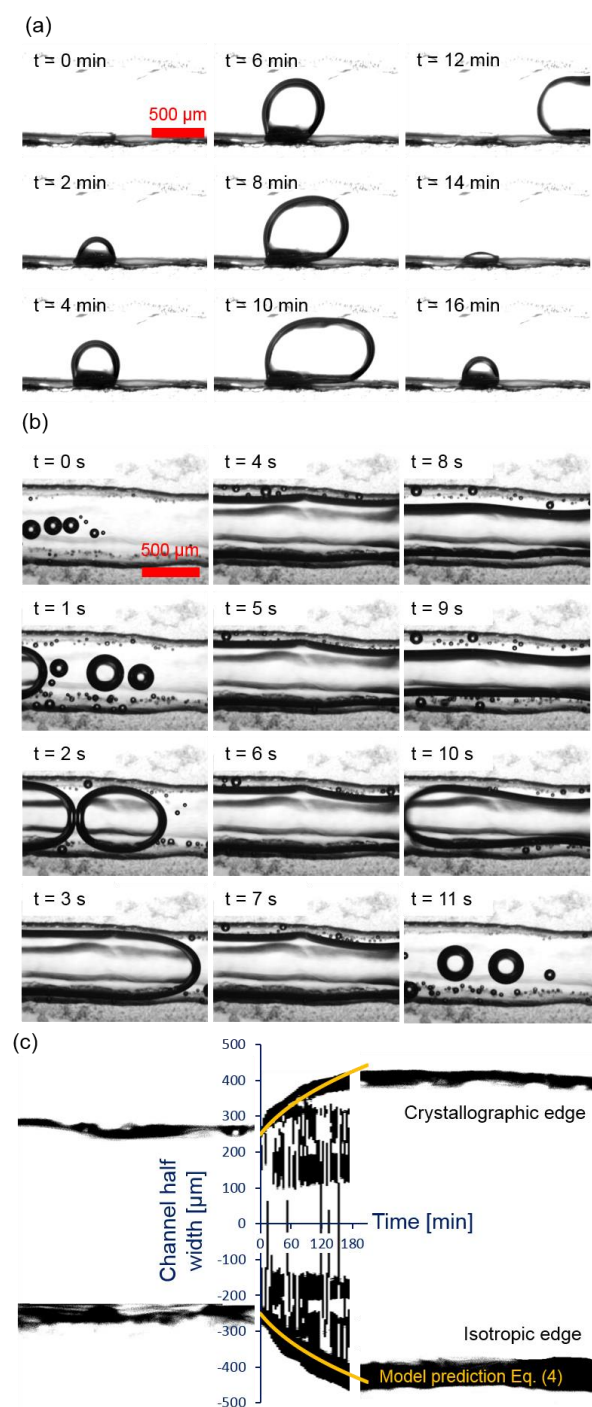
t = 3 s   t = 7 s   t = 11 s

(c)

Fig. 4 Visualization and quantification of dissolution dynamics in an initially 500μm wide channel under acidic flow conditions. Dilute, 0.1% HCl brine injection at 2 m/day (a) and 1% HCl brine injection at 100 m/day (b). The initial and final channel widths and rate at which the channel width increased over the course of three hours of 1% HCl brine injection at 100 m/day velocities (c). The predicted channel growth is superimposed on the local cross-sectional slices of the channel over time.

Fig. 4c shows the channel at its initial (left) and final (right) stages, after three hours of 1% HCl brine injection, corresponding to reservoir-relevant conditions of Fig. 4b. As shown, the sharp
5 crystallographic edge is at the top and the rounded isotropic edge is at the bottom. The time-evolution of the channel width at the channel midpoint (15 mm from inlet) is plotted in the middle.

Specifically, image slices of the channel width at that location taken at two minute intervals are plotted vs. time. As shown, the
10 channel width increases over time in a decaying nonlinear fashion. The vertical lines between 0 and 180 minutes are a result of the nucleation, growth, and transport of CO_2 bubbles which were captured at that location. That is, these lines are simply artifacts resulting from image sections obtained while a
15 bubble was present. At locations upstream and downstream of the midpoint, similar dissolution dynamics were observed. Notably, the rate of dissolution was higher upstream than downstream, in keeping with expected transport limitation dynamics.
20 The simple straight-channel geometry enables an analytical prediction of the dissolution rate for comparison. Assumed here is a uniform dissolution rate across the three calcite surfaces that is proportional to the local velocity. The local velocity was defined as the injection flow rate, Q, divided by the instantaneous cross-
25 sectional area of the specific location along the channel, which was obtained through imaging. The resulting differential equation has the solution for channel width over time as follows:

$$l(t) = \left(3kQt + l_0^3\right)^{1/3} \qquad (4)$$

where the channel cross-sectional dimension as a function of time, $l(t)$, varies with a dissolution constant, k, flow rate, Q, and the
30 initial channel width, l_0.

These predicted channel dimensions are plotted versus time in Fig. 4c (overlaying the experimentally obtained image data). The dissolution constant used was $k = 0.0009$, specific to this location, initial acid concentration, channel geometry, and flow rate. The fit
35 with the experimental data is strong for both top and bottom edges. In particular, the fit with the isotropic edge (bottom in Fig. 4c) is best, as expected due to the abundance of exposed step nucleation sites available for reaction. Moreover, the simple analytical model does not account for crystal planes etc., and thus the channel width
40 on the crystallographically-defined plane (top in Fig. 4c) dissolved at a slower rate than the predicted rate for isotropic dissolution. In a natural heterogeneous reservoir, one could expect a combination of these dissolution rates (found here to differ by ~ 25%) to be active depending on the pore scale surfaces exposed.

45 **Two-dimensional micromodel experiments**

A fabricated two dimensional calcite micromodel is shown in Fig. 5. The device was initially filled with brine (dyed black to enhance contrast) under vacuum conditions before 1% HCl, 1.81M NaCl brine was injected to simulate acidizing processes. The
50 dissolution dynamics of the calcite matrix were observed at the macro- and pore-scales in real time using the USB microscope and brightfield microscope, respectively. Images were captured at a fixed location to monitor the dissolution of grains over time.

Fig. 5 Microfluidic network (micromodel) etched into a calcite crystal. The trigonal-rhombohedral structure of calcite is apparent as well as inherent natural fractures parallel to the crystal planes.

Fig. 6 shows preferential grain dissolution observed along the streamlines with high localized velocities of fresh acidic brine. At the pore scale, preferential dissolution about a single grain was also observed – that is, highly asymmetrical dissolution owing to (i) preferential flow along a given side of a grain, and/or (ii) the alignment of crystal planes with the exposed surface (similar to that observed in the straight channel case, Figs. 3 and 4). While direct measurements of local fluid velocities were not possible with this setup, the local velocities were approximated from the observed bubble velocities in the image sequences. Specifically, for flow about the grains in Fig. 6, average local velocities on the order of 175 μm/s are indicated on the isotropic surfaces, approximately four-fold higher than on the anisotropic surfaces. In Fig. 6 the dissolution of grains over time is delineated in red in the images and compiled in Fig. 6b. As shown, the isotropic edges were dissolved at much faster rates compared to regions in stagnant fluid, as seen in the resulting oblong triangular shape of the initially square grain.
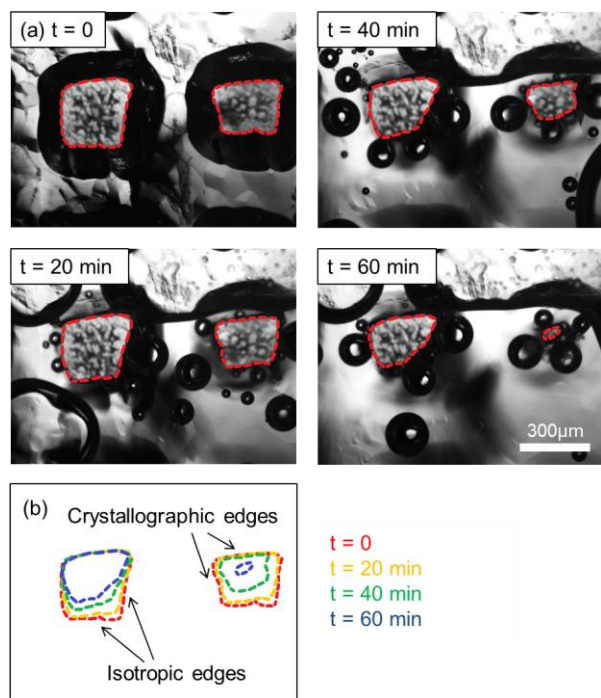

Fig. 6 Pore-scale dissolution of micromodel exposed to reservoir-relevant conditions near the well bore. (a) The pore scale dissolution imaged over time at 0, 20, 40, and 60 minutes with 1% HCl, 1.81M NaCl brine injection. (b) The transition from the initially square grain to an oblong triangular shape, with the most highly eroded sides being the isotropic edges in the high flow velocity region. Video is shown in the accompanying electronic supplementary information (ESI).

In contrast to the single channel case (Fig. 4), the dissolution dynamics within the micromodel are complicated by the coupling of pore sizes throughout the network and the local flow rate. That is, in the single channel case, the local velocity continuously and predictably *decreased* as channel size increased with dissolution. In the micromodel case, however, increased local dissolution along the more permeable flow paths *increases* local velocity and increases dissolution in turn. The result is a positive feedback, and

preferential flow and dissolution resulting in a highly heterogeneous erosion pattern. These dynamics are apparent at the micromodel scale, shown in Fig. 7.

The calcite micromodel was imaged over time with the colored fluid delineating the pore space and the light region indicating carbonate grains in Fig. 7. Binary images were created using ImageJ to distinguish between the pore space (black) and the grains (white). The initial matrix geometry of a calcite micromodel is shown at time t = 0, with the same micromodel after 15, 30, and 45 minutes of 1% HCl brine injection at near-wellbore flow rates of 100 m/day. It was observed that although the injected fluids initially penetrated the micromodel relatively evenly, non-uniform carbonate dissolution quickly created preferential flow paths, i.e., paths in which flow incurred the least resistance, and in turn increased the local dissolution. This effect is best characterized by the Damkohler number, $Da = E_f C_o^{m-1}/u$,[11] where, E_f is the reaction rate constant for the calcium carbonate – hydrochloric acid reaction, C_0 is the initial acid concentration, and $m=1$ is the order of the calcite – hydrochloric acid reaction. The experimental conditions of Fig. 7 corresponding to near-wellbore injection rates (~ 100 m/day) relate to a Damkohler number Da ~ 10^1, where conduit formation (or 'wormholing') can be expected.[20] Micromodels run at lower velocities (~ 1 m/day, corresponding to Da ~ 10^3) resulted in a more even dissolution front close to the injection site.
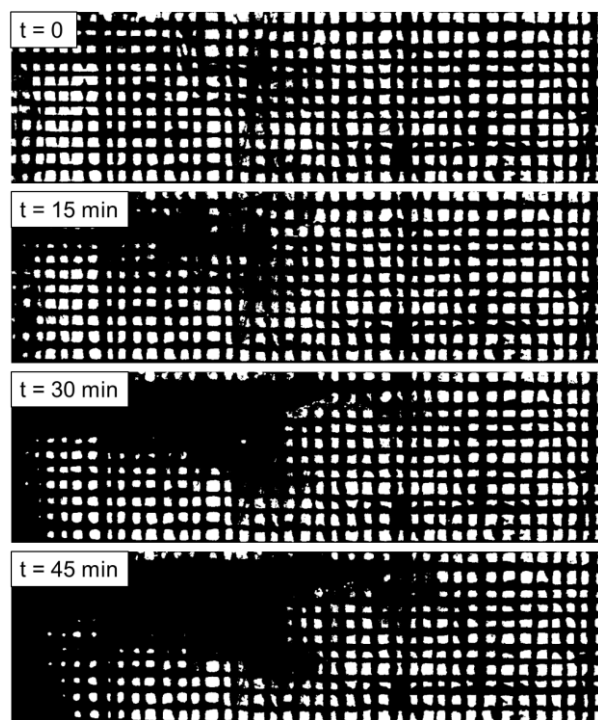

Fig. 7 Binary image of two dimensional calcite micromodel during flow experiments, with times indicated. The calcite matrix is shown in white and the pore space fluid included a black dye to enable imaging. The injection was at near-wellbore conditions, 1% HCl, 1.81M NaCl brine injection, corresponding to a Damkohler number, Da ~ 10. Preferential paths in the form of highly dissolved conduits were observed.

The change in matrix porosity over time generated from the binary macroscale images is plotted in Fig. 8, indicating an approximately linear trend with a correlation coefficient of $R^2 = 0.9517$. This result is in keeping with a constant flowrate of reactant (acid) that is fully utilized within the network. In addition, the nonlinear trend expected in the ideal single-channel case is not expected within a network due to the coupled influence of dissolution on pore size and local fluid velocity as noted earlier.
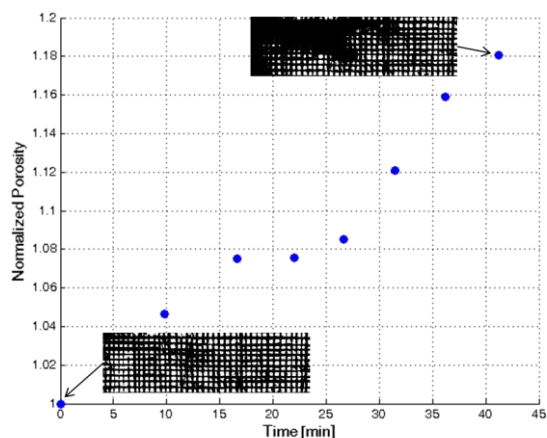

Fig. 8 Porosity (normalized against the initial porosity) of a typical two dimensional calcite micromodel over time as a result of acidic (1% HCl, 1.81M NaCl) brine injection at near well flow rates (~100m/day), representative images are shown inset.

The real-rock microfluidic approach developed in this work enables the direct visualization of pore-scale phenomena with representative fluid-solid interactions (e.g., wettability, reaction, etc.). The key advantage of this method is the ability to directly observe complex multiphase, multicomponent interactions between the various phases in real time, including the relevant chemical reactions which conventional micromodels could not replicate. While the simple acid dissolution applied here enabled validation of the method (both to an analytical model and known porous media reaction kinetics), the strength of the method is in testing/screening the influence on non-idealized systems typical of industry. Specifically, injected fluids are generally impure, complex mixtures for which the dissolution mechanics are not readily predictable. In such cases, microfluidic screening can provide rapid insight to previously inaccessible phenomena. In short, real-rock microfluidics can replicate real processes in the subsurface.

Real-rock microfluidics present some inherent limitations and challenges. The requirement for developing such devices hinges upon the existence of a crystalline form of the rock type of interest: common reservoir formations that present crystal forms include sandstones, limestones, and dolostones. Although these formations are globally ubiquitous, many other formations are of interest. Perhaps most notably shale formations – the source rock for much recent development in the US - are not well suited to this approach. Likewise reservoirs with a high degree of compositional heterogeneity are poor candidates for this approach. Specifically in the context of carbonate formations, the real-rock approach here is applicable to regions with microscale structure. Although such pore structures are typical of carbonate formations, they can also

have large voids not represented in the model. Fortunately, such voids lend themselves to reservoir simulation. Similar to previous glass and silicon micromodels, the influence of pore-scale heterogeneities such as the presence of clays cannot easily be included in the real-rock microfluidics approach presented here. Also on a practical level, real-rock microfluidics are one-use-only, that is, the chip is inherently altered/dissolved in the process. The experimental method is thus inherently fabrication intensive, although fortunately the method presented here is relatively simple (as compared to glass or silicon). Furthermore, microfluidic studies are currently confined to two dimensions, while natural flow generally occurs in three-dimensions. Notably planar platforms offer the unique advantage of direct, optical visualization of flow and phase phenomena at the pore-scale which would have been otherwise. Thus here, as with all two-dimensional micromodel approaches, there is a trade-off between pore-scale insight provided by the planar geometry and three-dimensional relevance, as outlined by Datta *et al*.[33]

In summary, real-rock microfluidics opens a window to improve our understanding of subsurface phenomena at the pore-scale, both mechanistically and chemically, and paves way for future studies related to harvesting the enormous resource potential in carbonate reservoirs. In the context of the Lab-on-a-Chip community, real-rock microfluidics opens the door to a vast array of opportunities in geology, reservoir engineering and earth sciences.

Conclusion

In this study, we present a real-rock micromodel approach whereby microfluidic channels are fabricated in a naturally occurring mineral substrate. The key advantage of this method is the ability to directly observe complex reservoir-relevant multiphase, multicomponent interactions in real time, including the relevant fluid-solid chemical reactions which conventional microfluidics/micromodels cannot replicate. The approach was applied to calcite dissolution – an industrially and environmentally important process worldwide. The microfluidic device, fabricated using calcite (calcium carbonate), is the first use of microfluidics that is chemically and geometrically representative of real rocks for study of subsurface phenomena. We demonstrated the dissolution of carbonate rock over time as a result of hydrochloric acid flow in conditions relevant to acidizing processes for reservoir stimulation. A single straight channel as well as a two dimensional porous network were used to demonstrate the device capabilities in visualizing the dissolution mechanics of calcium carbonate. Specifically, flow- and crystal orientation- directed preferential dissolution were observed, differing by 25% in dissolution rates, and compared well to an analytical solution. The real-rock micromodel successfully replicated wormhole generation in this process at reservoir-relevant conditions. Most importantly, this work provides the basis for future applications of real-rock microfluidics in understanding real processes in the subsurface. Specifically, the real-rock microfluidics approach can be applied to (i) study the fundamental fluid-rock interactions relevant to enhanced hydrocarbon recovery, and (ii) test/screen the influence

of industrially-relevant (impure) injection fluids in carbonate reservoir stimulation and CO_2 storage in saline aquifers.

Author Information and Notes

[a] *Department of Mechanical and Industrial Engineering, and Institute for Sustainable Energy, University of Toronto, Toronto, Canada. Tel: +1 (416) 978 1623; E-mail: sinton@mie.utoronto.ca*
[b] *Suncor Energy Inc., 150 6 Ave SW, Calgary, AB T2P 3Y7, Calgary, Canada.*

† Electronic Supplementary Information (ESI) available: See DOI:

Acknowledgements

References

1. Elkhoury, J. E., Ameli, P. & Detwiler, R. L. Dissolution and deformation in fractured carbonates caused by flow of CO2-rich brine under reservoir conditions. *Int. J. Greenh. Gas Control* **16,** S203–S215 (2013).

2. International Energy Agency. *World Energy Outlook.* (2006).

3. Arsalan, N., Palayangoda, S. S., Burnett, D. J., Buiting, J. J. & Nguyen, Q. P. Surface energy characterization of carbonate rocks. *Colloids Surfaces A Physicochem. Eng. Asp.* **436,** 139–147 (2013).

4. Nguyen, P., Fadaei, H. & Sinton, D. Microfluidics Underground: A Micro-Core Method for Pore Scale Analysis of Supercritical CO2 Reactive Transport in Saline Aquifers. *J. Fluids Eng.* **135,** 021203 (2013).

5. Jiang, Q., Yuan, J., Russel-Houston, J., Thornton, B. & Squires, A. Evaluation of Recovery Technologies for the Grosmont Carbonate Reservoirs. in *Proc. Can. Int. Pet. Conf.* 1–11 (Society of Petroleum Engineers, 2009). doi:10.2118/2009-067

6. Burrowes, R. A. *et al. Alberta's Energy Reserves 2010 and Supply/Demand Outlook 2011-2020 ST98- 2011.* (Energy Resources Conservation Board, 2011).

7. Schlumberger. *Middle East and Asia Reservoir Review.* (2009).

8. Leahy, M., Barden, J. L., Murphy, B. T., Slater-thompson, N. & Peterson, D. *International Energy Outlook 2013.* (2013).

9. Njiekak, G., Schmitt, D. R., Yam, H. & Kofman, R. S. CO2 rock physics as part of the Weyburn-Midale geological storage project. *Int. J. Greenh. Gas Control* **16,** S118–S133 (2013).

10. International Energy Agency. *World Energy Outlook.* (2008).

11. Wang, Y., Hill, a. D. & Schechter, R. S. The Optimum Injection Rate for Matrix Acidizing of Carbonate Formations. *Proc. SPE Annu. Tech. Conf. Exhib.* (1993). doi:10.2523/26578-MS

12. Hoefner, M. L. & Fogler, H. S. Pore evolution and channel formation during flow and reaction in porous media. *AIChE J.* **34,** 45–54 (1988).

13. Fredd, C. N. & Fogler, H. S. Alternative Stimulation Fluids and Their Impact on Carbonate Acidizing. *SPE J.* 34–41 (1998).

14. Lund, K., Fogler, H. S., McCune, C. C. & Ault, J. W. THE DISSOLUTION OF CALCITE IN HYDROCHLORIC ACID. *Chem. Eng. Sci.* **30,** 825–835 (1975).

15. Orr, F. M. Onshore geologic storage of CO2. *Science* **325,** 1656–1658 (2009).

16. Bickle, M. J. Geological carbon storage. *Nat. Geosci.* **2,** 815–819 (2009).

17. Bachu, S. & Adams, J. J. Sequestration of CO2 in geological media in response to climate change: capacity of deep saline aquifers to sequester CO2 in solution. *Energy Convers. Manag.* **44,** 3151–3175 (2003).

18. Gunter, W. D., Bachu, S. & Benson, S. The role of hydrogeological and geochemical trapping in sedimentary basins for secure geological storage of carbon dioxide. *Geol. Soc. London, Spec. Publ.* **233,** 129–145 (2004).

19. Matter, J. M. & Kelemen, P. B. Permanent storage of carbon dioxide in geological reservoirs by mineral carbonation. *Nat. Geosci.* **2,** 837–841 (2009).

20. Fredd, C. N. & Fogler, H. S. Influence of transport and reaction on wormhole formation in porous media. *AIChE J.* **44,** 1933–1949 (1998).

21. Whitesides, G. M. The origins and the future of microfluidics. *Nature* **442,** 368–373 (2006).

22. De Haas, T. W., Fadaei, H. & Sinton, D. Laminated thin-film Teflon chips for petrochemical applications. *Lab Chip* **12,** 4236–4239 (2012).

23. De Haas, T. W., Fadaei, H., Guerrero, U. & Sinton, D. Steam-on-a-chip for oil recovery: the role of alkaline additives in steam assisted gravity drainage. *Lab Chip* **13,** 3832–9 (2013).

24. Sell, A., Fadaei, H., Kim, M. & Sinton, D. Microfluidic Approach for Reservoir-Specific Analysis. *Environ. Sci. Technol.* **47,** 71–78 (2013).

25. Kim, M., Sell, A. & Sinton, D. Aquifer-on-a-Chip: understanding pore-scale salt precipitation dynamics during CO2 sequestration. *Lab Chip* **13,** 2421–2662 (2013).

26. Fadaei, H., Shaw, J. M. & Sinton, D. Bitumen–Toluene Mutual Diffusion Coefficients Using Microfluidics. *Energy & Fuels* **27,** 2042–2048 (2013).

27. Mostowfi, F., Molla, S. & Tabeling, P. Determining phase diagrams of gas-liquid systems using a microfluidic PVT. *Lab Chip* **12,** 4381–4387 (2012).

28. Song, W., Fadaei, H. & Sinton, D. Determination of Dew Point Conditions for CO 2 with Impurities Using Microfluidics. *Environ. Sci. Technol.* **48,** 3567–3574 (2014).

29. Buchgraber, M., Al-Dossary, M., Ross, C. M. & Kovscek, a. R. Creation of a dual-porosity micromodel for pore-level visualization of multiphase flow. *J. Pet. Sci. Eng.* **86-87,** 27–38 (2012).

30. Buchgraber, M., Kovscek, A. R. & Castanier, L. M. A Study of Microscale Gas Trapping Using Etched Silicon Micromodels. *Transp. Porous Media* **95,** 647–668 (2012).

31. Luo, P. & Machel, H. G. Pore Size and Pore Throat Types in a Heterogeneous Dolostone Reservoir , Devonian Grosmont Formation , Western Canada Sedimentary Basin 1. *Am. Assoc. Pet. Geol. Bull.* **11,** 1698–1720 (1995).

32. Brantley, S. L., Kubicki, J. D. & White, A. F. *Kinetics of Water-Rock Interaction*. (Springer, 2008).

33. Datta, S. S., Ramakrishnan, T. S. & Weitz, D. A. Mobilization of a trapped non-wetting fluid from a three-dimensional porous medium. *Phys. Fluids* **26,** 022002 (2014).

Lab on a Chip Accepted Manuscript